Inner-layer intensities for the flat-plate turbulent boundary layer combining a predictive wall-model with large-eddy simulations

M. Inoue, R. Mathis, I. Marusic, and D. I. Pullin

Citation: Phys. Fluids **24**, 075102 (2012); doi: 10.1063/1.4731299
View online: http://dx.doi.org/10.1063/1.4731299
View Table of Contents: http://pof.aip.org/resource/1/PHFLE6/v24/i7
Published by the American Institute of Physics.

Related Articles

Lagrangian evolution of the invariants of the velocity gradient tensor in a turbulent boundary layer
Phys. Fluids 24, 105104 (2012)

Effects of moderate Reynolds numbers on subsonic round jets with highly disturbed nozzle-exit boundary layers
Phys. Fluids 24, 105107 (2012)

Particle transport in a turbulent boundary layer: Non-local closures for particle dispersion tensors accounting for particle-wall interactions
Phys. Fluids 24, 103304 (2012)

Convection and reaction in a diffusive boundary layer in a porous medium: Nonlinear dynamics
Chaos 22, 037113 (2012)

Symmetry analysis and self-similar forms of fluid flow and heat-mass transfer in turbulent boundary layer flow of a nanofluid
Phys. Fluids 24, 092003 (2012)

Additional information on Phys. Fluids

Journal Homepage: http://pof.aip.org/
Journal Information: http://pof.aip.org/about/about_the_journal
Top downloads: http://pof.aip.org/features/most_downloaded
Information for Authors: http://pof.aip.org/authors

ADVERTISEMENT

Downloaded 22 Oct 2012 to 128.250.144.147. Redistribution subject to AIP license or copyright; see http://pof.aip.org/about/rights_and_permissions

PHYSICS OF FLUIDS **24**, 075102 (2012)

Inner-layer intensities for the flat-plate turbulent boundary layer combining a predictive wall-model with large-eddy simulations

M. Inoue,[1,a)] R. Mathis,[2] I. Marusic,[2] and D. I. Pullin[1]
[1]*Graduate Aerospace Laboratories, California Institute of Technology, Pasadena, California 91125, USA*
[2]*Department of Mechanical Engineering, University of Melbourne Parkville, Victoria 3010, Australia*

(Received 6 March 2012; accepted 31 May 2012; published online 2 July 2012)

Time series velocity signals obtained from large-eddy simulations (LES) within the logarithmic region of the zero-pressure gradient turbulent boundary layer over a smooth wall are used in combination with an empirical, predictive inner-outer wall model [I. Marusic, R. Mathis, and N. Hutchins, "Predictive model for wall-bounded turbulent flow," Science **329**, 193 (2010)] to calculate the statistics of the fluctuating streamwise velocity in the inner region. Results, including spectra and moments up to fourth order, are compared with equivalent predictions using experimental time series, as well as with direct experimental measurements at Reynolds numbers $Re_\tau = 7300$, 13 600, and 19 000. The LES combined with the wall model are then used to extend the inner-layer predictions to Reynolds numbers $Re_\tau = 62\,000$, 100 000, and 200 000 that lie within a gap in $\log(Re_\tau)$ space between laboratory measurements and surface-layer, atmospheric experiments. The present results support a loglike increase in the near-wall peak of the streamwise turbulence intensities with Re_τ and also provide a means of extending LES results at large Reynolds numbers to the near-wall region of wall-bounded turbulent flows. © *2012 American Institute of Physics*. [http://dx.doi.org/10.1063/1.4731299]

I. INTRODUCTION

It has long been known that wall-bounded turbulent flows at moderate to large Reynolds number contain an extremely large range of eddy length scales. For the flat plate turbulent boundary layer, one measure of this is the friction Reynolds number $Re_\tau \equiv u_\tau\, \delta/\nu$, where $u_\tau \equiv \sqrt{\tau_w/\rho}$ is the friction or inner velocity scale and $\delta, \tau_w, \nu, \rho$ are the boundary layer thickness, wall shear stress, fluid kinematic viscosity, and density, respectively. Recent experimental studies at large Re_τ, however, have suggested that δ is not itself the largest dynamically active length scale in the zero-pressure gradient turbulent boundary layer (ZPGTBL). Convincing evidence[1–6] indicates that there exists very large-scale motions (VLSMs) or "superstructures" with scales of order $15-20\delta$ within the outer logarithmic part of the turbulent boundary layer. It is hypothesized that these elongated structures are slightly inclined to the horizontal and may be accompanied by large-scale counter-rotating roll-like modes; see Mathis *et al.*[7] for a summary and discussion.

It has also been highlighted that the dynamical influence of the large-scale events extends to the wall where they affect the small-scale, near-wall fluctuations, in a significant way. Metzger and Klewicki[8] showed that long wavelength motions, which scale on outer variables, have a significant effect on second, third, and fourth moments of the turbulence near the wall.

The studies of Abe *et al.*[9] and Hutchins and Marusic[6] have clearly indicated that the large-scale motions are felt all the way down to the wall, as a strong imprint (consistent with the attached eddy

---

[a)] Electronic mail: minoue@caltech.edu.

© 2012 American Institute of Physics

Downloaded 22 Oct 2012 to 128.250.144.147. Redistribution subject to AIP license or copyright; see http://pof.aip.org/about/rights_and_permissions

hypothesis of Townsend[10]). Furthermore, Mathis *et al.*[11] have shown that their influence is not simply a superposition, but also that these large-scale motions, associated with the log-region, substantially amplitude modulate the near-wall small-scale structures. In their work, Mathis *et al.*[11] developed a mathematical tool to quantify the degree of modulation. Recently, Marusic *et al.*[12] and Mathis *et al.*[7] incorporated these ideas into an algebraic model that enables the prediction of near-wall statistics of turbulent streamwise velocity fluctuations using a single-point log-layer time-series signal as an input. Further details on this model are given in Sec. II A.

Investigations using either direct numerical simulation (DNS) or large-eddy simulations (LES) of near-wall turbulence – for long-domain boundary layers at the largest laboratory Reynolds numbers presently achievable or for atmospheric boundary layers – have been hampered owing to the presence of small yet dynamically important anisotropic near-wall structures. The requirements for resolving both near-wall small eddies and large-scale structures severely limit the range of Re_τ accessible by both DNS and wall-resolved LES (in which near-wall structures are at least partially resolved). A further requirement is the capability of capturing variations $\sim O(\log(Re_\tau))$ in some important quantities, such as the wall skin-friction coefficient for smooth-wall flow. An alternative to wall-resolved LES is the use of wall-models specifically constructed to represent the effect of near-wall anisotropic eddies (see Piomelli[13] for a review). While a principal objective of wall-modeled LES is to avoid the necessity of explicit resolution of near-wall turbulent structures, this comes with the price that some flow properties – such as the detailed near-wall statistics and their dependence on the presence of large-scales in the outer flow – cannot be investigated directly. We address this issue presently.

The main purpose of the present work is to examine the near-wall region of zero-pressure gradient turbulent boundary layer using a combination of wall-modeled LES coupled to a predictive wall model[7,12] at Reynolds numbers which have been not yet accessible, by either numerical simulation or laboratory experiment. Specifically, we utilize a wall-modeled LES (Ref. 14) to provide the large-scale log-region velocity time series as the input to the predictive near-wall model of Marusic *et al.*[12] and Mathis *et al.*[7] The combined LES and predictive inner-outer model potentially extends the LES capability to high Reynolds numbers, spanning the gap between laboratory turbulent boundary-layers and atmospheric surface-layers. This allows us to address some open questions regarding the large-scale effects on the near-wall statistics and their dependency on Reynolds number. For instance, the existence of an outer peak in the turbulent fluctuations profile remains controversial, and it would be only evident at very high Reynolds number.[15,16]

Brief accounts of both the predictive inner-outer model and subgrid-scale (SGS) model employed in the current LES are described in Sec. II. This is followed by an account of the LES in Sec. III. Discussion of results is found in Secs. IV and V before the conclusions in Sec. VI.

II. WALL MODEL DESCRIPTION

From the preceding discussions it should be clear that two different "wall models" are being considered here. Since these models are independent and have different functions, for the purposes of clarity we distinguish these as follows. Also see Figure 1. The first is the predictive inner-outer wall model of Mathis *et al.*,[7] described in Sec. II A. We will refer to this as the "PIO wall model." The second is the "LES wall model," described in Sec. II B. The purposes of this LES model is to avoid the necessity of resolving the inner wall layer while still providing an estimation of the wall friction velocity. Also, it gives a boundary condition for the outer-flow LES at a "virtual" wall located at a fixed height from the actual wall. In the present work, the LES provides a velocity signal as an input to the PIO wall model. It should be emphasized that the LES wall-model is independent of and does not require feedback from the PIO wall model, and vice versa.

A. Predictive inner-outer model

Marusic *et al.*[12] and Mathis *et al.*[7] proposed a quantitative model to reconstruct the fluctuating streamwise velocity field, $u_p^+(z^+, t)$, in the near-wall region, based on a single point observation of

Downloaded 22 Oct 2012 to 128.250.144.147. Redistribution subject to AIP license or copyright; see http://pof.aip.org/about/rights_and_permissions

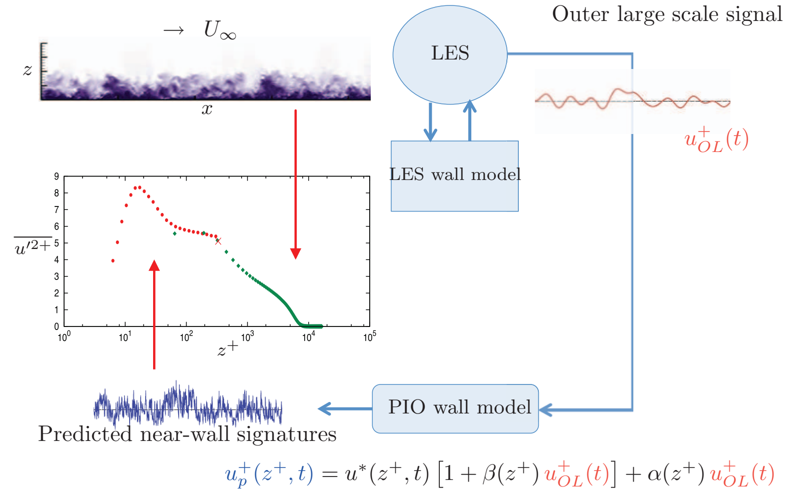

FIG. 1. Schematic description of two "wall models."

the large-scales in the log-region, $u^+_{OL}(t)$,

$$u^+_p(z^+, t) = u^*(z^+, t)\left[1 + \beta(z^+)\, u^+_{OL}(t)\right] + \alpha(z^+)\, u^+_{OL}(t), \tag{1}$$

where u^+_p is the predictive time-series at z^+. The time-series u^* represents a statistically "universal" signal of the small-scales at z^+ that would exist in the absence of any inner-outer interactions. The quantities $\alpha(z^+)$ and $\beta(z^+)$ are, respectively, the superposition and modulation coefficients. The parameters u^*, α, and β are determined experimentally during the calibration of the model and are hypothesized to be Reynolds number independent. Note that the model in Eq. (1) consists of two parts. The first part of the equation models the amplitude modulation effect of the small-scales (u^*) by the large-scale motions (u^+_{OL}). The second term models the linear superposition of the large-scale events felt at a given wall-normal position z^+. In order to apply (1), u_τ must be known.

The only required input signal to the model is the large-scale fluctuating velocity signal from the log-region, $u^+_{OL}(t)$, taken at the normalized wall-normal position where the calibration experiment was conducted, which is $z^+_O = \sqrt{15\, Re_\tau}$, the approximate geometric center of the log-region.[11] The large-scales signal is obtained by filtering first the raw signal to retain only length scales greater than a streamwise wavelength $\lambda^+_x > 7000$ (using Taylor's hypothesis). Then, a spatial shift is applied to account for the mean inclination angle of the large-scale structures. The final step is to retain the Fourier phase information of the large-scale component used during the calibration of the model. See Mathis *et al.*[7] for further details about the model and specific values of the parameters in Eq. (1).

Here the distance from the wall, z, and the streamwise velocity component, u, are normalized by inner-scale variables so that $z^+ \equiv z\, u_\tau/\nu$ and $u^+ \equiv u/u_\tau$. Also, u^* is normalized against u_τ.

B. LES and LES wall model

Presently, we use LES of the zero-pressure gradient, smooth-wall, flat plate, turbulent boundary layer to provide a rake of velocity time series obtained at $z^+ \approx z^+_O$ as the raw signal input u^+_O to the PIO wall model, that is the signal from which $u^+_{OL}(t)$ is obtained. Equation (1) then supplies a time series $u^+_p(z^+, t)$ at each z^+ from which both wall-normal variation of several moments of the probability-density function of the steamwise fluctuating velocity can be obtained as well as longitudinal spectra (using a local Taylor hypothesis) within a region that is inaccessible to the LES. The LES is based on an extension of turbulent channel flow LES (Ref. 17) to the zero-pressure gradient, developing turbulent boundary layer.[14]

Chung and Pullin[17] developed a LES approach for near-wall flows based on combining the stretched-vortex SGS model with a tailored wall model. Their LES wall model begins with an

Downloaded 22 Oct 2012 to 128.250.144.147. Redistribution subject to AIP license or copyright; see http://pof.aip.org/about/rights_and_permissions

analytic integration of the streamwise momentum equation across a constant-thickness, wall-adjacent layer. Using inner-scaling to reduce the unsteady term, this leads to an ordinary-differential equation (ODE) at each point on the wall for the wall-normal gradient of xy-plane filtered streamwise velocity $\eta(x, y, t)_w \equiv \partial\tilde{u}/\partial z$ where (x, y, z) are streamwise, spanwise, and wall-normal co-ordinates, respectively. This ODE contains the actual no-slip wall boundary condition together with inertial transport and viscous source terms that can be obtained from the LES, thus coupling the ODE to the outer LES while providing dynamical computation of the local wall shear stress, $\tau_w = \mu\, \eta_w$, and hence the local friction velocity, $u_\tau^2 \equiv \nu\eta_w$, at all points on the wall.

Next, Chung and Pullin[17] apply the stretched vortex SGS model within a near-wall region where it is assumed that the subgrid vortex elements represent attached vortices in the presence of the wall with assumed scaling that is linearly proportional to their distance from the wall. This is intended to capture the principal dynamical behavior of longitudinal vortices in wall-normal transport of streamwise momentum. An integration then leads to a "log-like" relationship for the "filtered" streamwise velocity in an inner, modeled layer bounded above by a virtual wall at $z = h_0$ and below by the actual no-slip wall at $z = 0$,

$$\tilde{u}(z^+) = u_\tau\left(\frac{1}{\mathcal{K}_1}\log\left(\frac{z^+}{h_\nu^+}\right) + B\right), \quad B = h_\nu^+ - \frac{\log h_\nu^+}{\mathcal{K}_1}, \tag{2a}$$

$$\mathcal{K}_1(x, y, t) = \frac{\gamma_{\mathrm{II}} K^{1/2}}{2\,(-T_{xz}/u_\tau)}, \tag{2b}$$

where $\mathcal{K}_1(x, y, t)$ is a Kármán-like "constant" and T_{ij} is the subgrid stress tensor. They can be calculated dynamically in the LES and $\gamma_{\mathrm{II}} = \sqrt{2}/\pi$ is a mixing constant obtained using Townsend's structure parameter,[17] K is the local SGS kinetic energy, and $h_\nu^+ = 10.23$ is an empirical parameter that appears as an integration constant in obtaining (2a). Since u_τ is known from the numerical solution of the ODE and $\mathcal{K}_1(x, y, t)$ is provided by the LES, then (2) can be used to provide a slip-velocity boundary condition, $\tilde{u}(h_0^+)$ at $z = h_0$, for the outer-flow LES. Other boundary conditions are $\tilde{w} = 0$ and $\tilde{v}$ obtained from the continuity equation. Using this composite model, LES of channel flow at Re_τ up to 2×10^7 were reported,[17] while Inoue and Pullin[14] extended the model to performed LES of ZPGTBL at Re_θ up to $O(10^{12})$.

III. SIMULATION DETAILS

A. Numerical method

The fractional-step method[18] is used to solve the three-dimensional, incompressible, LES versions of the Navier-Stokes and continuity equations with periodic boundary condition in the spanwise or y-direction. Explicit, fourth-order finite differences on a staggered grid are used to approximate x and z-derivatives, while a Fourier spectral method is utilized for y-derivatives. Conservation of kinetic energy in the inviscid limit is achieved by the numerical scheme with the use of staggered grids.[19] Scalable parallelization is achieved using a message passing interface. Details of the algorithm are described in Inoue and Pullin.[14] The inflow generation scheme of Lund *et al.*[20] combined with the mirroring method proposed by Jewkes *et al.*[21] was used for all LES. This is shown to almost completely remove the spatially quasi-periodic effect in the overall LES.[14] It may also allow shorter domain sizes in both DNS and LES of spatially developing boundary-layer flows, although not discussed in this paper.

B. LES performed

The present LES, summarized in Table II, were designed to match experimental conditions reported[7,11] based on $Re_\theta = \theta U_\infty/\nu$, where θ is the local momentum thickness and U_∞ is the free-stream velocity. The grid is uniform, $\Delta_x = \Delta_y = 3\Delta_z$, throughout the simulation domain. The raised wall is at $h_0 = 0.18\,\Delta_z$ for all LES independent of resolution. To capture the physics of long large-scale structures, we use long streamwise domains with $L_x/\delta_0 = 72$, where δ_0 is the inlet boundary-layer thickness. LES were performed in a domain $(L_x/\delta_0, L_y/\delta_0, L_z/\delta_0) = (72, 6, 4)$. The

Downloaded 22 Oct 2012 to 128.250.144.147. Redistribution subject to AIP license or copyright; see http://pof.aip.org/about/rights_and_permissions

TABLE I. Simulation parameters and some resulting quantities. Inflow velocity is a re-scaled velocity field taken from $x_{\mathrm{ref}} = 0.8L_x$. $(L_x/\delta_0,\ L_y/\delta_0,\ L_z/\delta_0) = (72,\ 6,\ 4)$, where δ_0 is the inlet boundary-layer thickness. The velocity signal was taken from $x_{\mathrm{stat}} = 0.75L_x$ except for case 62k-τ, where $x_{\mathrm{stat}} = 0.45L_x$. dt is a time step size, $T^+ \equiv T\,u_\tau^2/\nu$ is the normalized time interval over which the velocity signal was obtained. $Re_{\tau,\,99} = u_\tau \delta_{99}/\nu$ and δ_{99} is the 99% boundary layer thickness. δ_c is the boundary layer thickness defined in Perry *et al.*[22] Kármán constant $\overline{\mathcal{K}_1}$ from (2b) and an additive constant B from (2a).

Case	N_x	N_y	N_z	dt	T^+	$Re_{\tau,\,99}$	δ_{99}	δ_c	u_τ	$\overline{\mathcal{K}_1}$	B
7.3k-θ	768	64	128	0.08	1.44×10^6	6.89×10^3	1.67	1.74	0.0338	0.397	4.38
13.6k-θ	768	64	128	0.08	2.07×10^6	1.25×10^4	1.63	1.76	0.0321	0.389	4.25
19k-θL	768	64	128	0.08	2.08×10^6	1.62×10^4	1.61	1.76	0.0313	0.386	4.21
19k-θH	1152	96	192	0.06	1.41×10^6	1.60×10^4	1.60	1.85	0.0313	0.389	4.25
62k-τ	1728	144	288	0.04	8.72×10^5	5.44×10^4	1.31	1.55	0.0283	0.382	4.15
100k-τ	2304	192	384	0.03	1.21×10^6	9.96×10^4	1.47	1.77	0.0271	0.381	4.12
200k-τ	3072	256	512	0.015	1.00×10^6	2.00×10^5	1.49	1.80	0.0257	0.386	4.21

LES provided a set of N_y velocity-time signals $u^+_{OL}(t)$, each at $z^+ = z^+_O$, across the spanwise extent of the LES domain. Since z^+_O did not fall on a grid point, fourth-order interpolation was used.

It should be noted that grid resolutions here are chosen such that z^+_O will be located at approximately $z_O \approx 5\,\Delta z/2$ (third wall-normal grid point) so as to minimize the effect of the under-resolved region close to the virtual wall where the LES wall-model provides a slip velocity as a boundary condition. An exception is case 19k-θL whose results show some effect of resolution (see Figure 8). Since z^+_O is fixed in inner scaling, then with the present uniform-grid LES and with a maximum of order 400 grid-points in the wall-normal direction this requirement limits presently attainable values of Re_τ, for the application of the current LES combined with the PIO wall model, to $Re_\tau = 2.0 \times 10^5$. We will subsequently refer to two sets of LES as intermediate (7.3k-θ, 13.6k-θ, 19k-θL,H of Table I) and large (62k-τ, 100k-τ, 200k-τ) Reynolds number, respectively. It should be emphasized that due to the above requirement to resolve the log-layer wall-normal location $z^+_O = \sqrt{15 Re_\tau}$, the grid point resolution used in the present PIO-LES model is rather more severe than the requirement of wall-modeled LES given by Chapman[25] or Choi and Moin.[26]

Each LES was run for 3-4 free-stream particle transit times through the domain, until statistical steady state was achieved, prior to the commencement of data sampling to calculate both time-averaged quantities and also the required velocity time series. Values of the LES sampling time period, $T^+ \equiv T\,u_\tau^2/\nu$, normalized on the wall-unit time ν/u_τ^2 are shown in Table I, which also lists some integral quantities. We note that the LES does not resolve the viscous, wall-time scale ν/u_τ^2.

The time series as input to the PIO model were obtained by sampling at every LES time step, Δt. Since for the present LES, $\Delta x = 3\,\Delta z$, then taking $\lambda^+_x \equiv \Delta x\, u_\tau/\nu$ and $\Delta z = \delta/N_\delta$, where N_δ is the number of grid points across the boundary layer, then gives, for the present LES, $\lambda^+_x = 3\,Re_\tau/N_\delta$. Typically, $N_\delta \approx N_z/3$ and the values displayed in Table I then show that $\lambda^+_x \leq 7000$ for the present LES as required by the PIO model.

C. Skin friction and mean velocity profiles

The variation of U_∞/u_τ versus Re_θ along the streamwise direction for intermediate Reynolds number is shown in Figure 2. Also shown are experimental measurements[7] and the semi-empirical Coles-Fernholz relation.[27] The wall-friction velocity u_τ and, therefore, the wall shear stress are provided directly from the ODE incorporated in the LES wall model. The S-factor profiles show a hill or bump after the inlet, also seen in DNS studies,[28] which is perhaps the effect of non-equilibrium following inlet as a result of the recycling procedure.[21,29,30] Note that the rake of velocity time series is taken well downstream of the hill where the effect of the inflow generation method is not visible. Our results over-estimate the S-factor of the experimental measurements by about 1.5%. Meanwhile the Coles-Fernholz gives a reasonable representation of the LES variation of U_∞/u_τ across those sections of our Re_θ range, where the boundary layer appears to be in equilibrium.

Downloaded 22 Oct 2012 to 128.250.144.147. Redistribution subject to AIP license or copyright; see http://pof.aip.org/about/rights_and_permissions

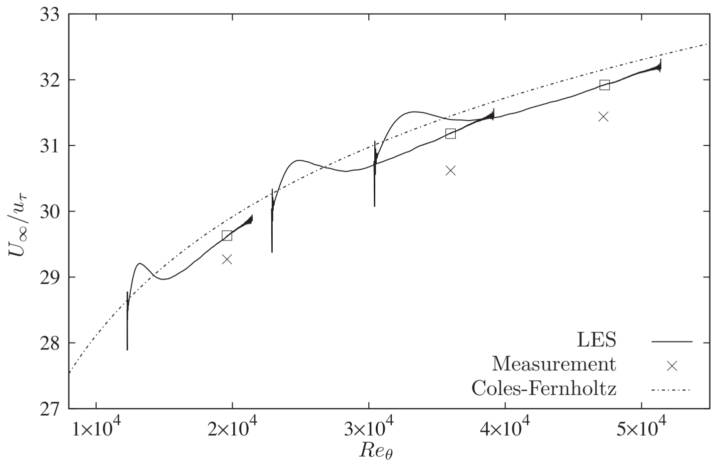

FIG. 2. Reynolds number dependency of U_∞/u_τ for cases 7.3k-θ, 13.6k-θ, and 19k-θH. Solid lines; LES results, each line corresponds to each simulation case. □: locations where the velocity time series is taken. ×: corresponding experimental measurements.[7] Dotted-dashed line: Coles-Fernholtz relation.[27]

It is evident from Table II that there are small but systematic differences in Re_τ between the present LES and experiment at matched Re_θ. It is well known that the boundary-layer thickness δ can be a poorly conditioned quantity as it depends on the measurement of a small velocity difference and various definitions exist. Presently, we use both a 99% velocity thickness δ_{99}, with $Re_{\tau,\,99} \equiv \delta_{99}\, u_\tau/\nu$, and also a thickness δ_c, based on a modified Coles law of the wake fit,[22] with $Re_{\tau,\,c} \equiv \delta_c\, u_\tau/\nu$. Values of $Re_{\tau,\,c}$ obtained independently from both LES and experiment are reasonably closely matched. See Table II for integral quantities of each simulation case and its corresponding experimental measurements.

Figure 3 shows LES mean velocity profiles in inner-scaling, $\overline{u^+} = \overline{u}/u_\tau$, for all Reynolds numbers compared with experimental measurements where available. LES captures the mean velocity profile reasonably accurately. We remark that the mismatch seen in the case 62k-τ is affected by the difference in Re_θ between the LES result (1.71×10^5) and corresponding measurements (1.56×10^5). The symbol "×" indicates the wall-normal location ($z_O^+ \approx \sqrt{15\, Re_\tau}$) where the large-scale velocity signal, $u_{OL}^+(t)$, is measured in LES. Although small, there seems to be a drop off in $\overline{u^+}$ towards the virtual wall. We interpret this as the influence of a logarithmic-layer mismatch.[31]

TABLE II. Reynolds number and ratio U_∞/u_τ for each LES and corresponding experiments.[7,11,23,24] S-factor; $S \equiv U_\infty/u_\tau$. $Re_\theta = U_\infty\theta/\nu$ and θ is the momentum thickness. $Re_{\tau,\,c} = u_\tau\delta_c/\nu$ is a Reynolds number based in boundary layer thickness δ_c.

Case	U_∞/u_τ	Re_θ	$Re_{\tau,\,c}$	$Re_{\tau,\,99}$
7.3k-θ	29.6	1.97×10^4	7.19×10^3	6.89×10^3
Exp	29.3	1.96×10^4	7.34×10^3	
13.6k-θ	31.2	3.60×10^4	1.34×10^4	1.25×10^4
Exp	30.6	3.60×10^4	1.36×10^4	
19k-θL	31.9	4.73×10^4	1.77×10^4	1.62×10^4
19k-θH	31.9	4.73×10^4	1.85×10^4	1.60×10^4
Exp	31.4	4.72×10^4	1.88×10^4	
62k-τ	35.3	1.71×10^5	6.43×10^4	5.44×10^4
Exp*	35.8	1.56×10^5	6.10×10^4	
100k-τ	36.9	3.22×10^5	1.20×10^5	9.96×10^4
200k-τ	38.9	6.65×10^5	2.42×10^5	2.00×10^5

Downloaded 22 Oct 2012 to 128.250.144.147. Redistribution subject to AIP license or copyright; see http://pof.aip.org/about/rights_and_permissions

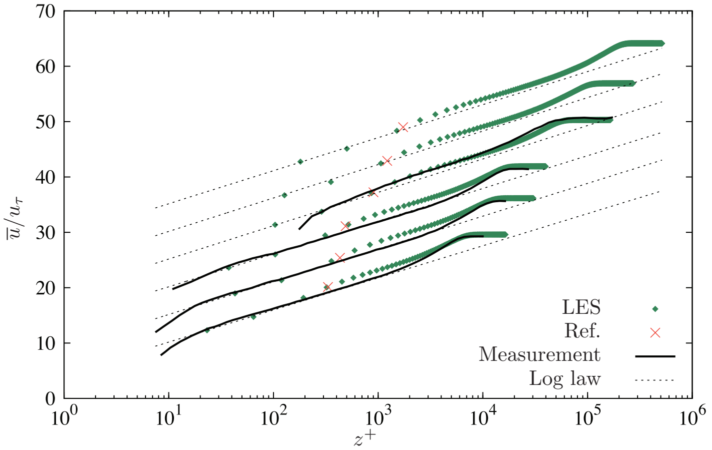

FIG. 3. Mean velocity profile for cases 7.3k-θ, 13.6k-θ, 19k-θH, 62k-τ, 100k-τ, and 200k-τ (from bottom to top). The experimental measurements at $Re_\tau = 7300$, 13 600, and 19 000 are from Mathis *et al.*,[7] and that at $Re_\tau = 62\,000$ is from Winkel *et al.*[24] The symbol "×" marks the location of where the large-scale component is measured. Profiles are displaced 5 units of $\overline{u}/u_\tau$ for clarity. Dashed-lines are log law using $\overline{\mathcal{K}_1}$ from (2b) and an additive constant B from (2a). Also see Table I.

IV. RESULTS AT INTERMEDIATE REYNOLDS NUMBERS

The velocity signals recorded in LES are now filtered to extract the large-scale fluctuating velocity $u^+_{OL}(t)$, an input to the predictive inner-outer model. In Secs. IV A–IV D, we discuss our observations of the predicted statistics, including spectra and some higher order moments within the inner region. The effects of resolution and the length of velocity time series are also discussed. We will refer to three distinct type of results: direct experimental measurements (Exp), inner-layer predictions obtained using the PIO model with $u^+_{OL}(t)$ provided by experiment (Exp-PIO) and inner-layer predictions obtained using the PIO model with $u^+_{OL}(t)$ provided by LES (LES-PIO).

A. Streamwise turbulent intensity

Figure 4 shows a comparison of the predicted streamwise turbulent intensity profile, LES-PIO, against experimental measurement (Exp) and prediction (Exp-PIO). Also included in Figure 4 is the turbulent intensity profile from LES over $z^+ > h^+_0$ containing SGS corrections to the resolved-flow calculated as $\overline{u'^2} = \overline{\widetilde{u}'\widetilde{u}'} + \overline{T_{xx}}$. The predicted LES-PIO $u'_{\rm rms}/u_\tau = \sqrt{\overline{u'^2}/u^2_\tau}$ profiles capture the essential features of the energy, including the slight increase of the near-wall peak with increasing Re_τ. The LES is seen to underestimate the intensity in the outer-region. This comes from the fact that not all scales are resolved with LES, which led to a slight underestimation of the turbulent intensity due to the missing small-scale energy content in the outer-region (which has a small, but noticeable, contribution). However, since only the large-scale component is needed for the PIO model, this does not affect the prediction. Furthermore, the good agreement between LES-PIO and Exp-PIO results demonstrates the capabilities of LES to capture accurately the large-scales required as input to the PIO model. This lends support toward the direct use of the PIO model in conjunction with, or instead of, the LES wall model.

B. Longitudinal spectra of streamwise velocity

Figure 5 shows the pre-multiplied energy spectra of the streamwise velocity fluctuations, $k_x\Phi_{uu}/u^2_\tau$, for the resolved velocity signal (u^+_O, i.e., not filtered) from LES and experiment at $Re_\tau \approx 7300$, 13 600, and 19 000, all at $z^+ \approx z^+_O$. It is clear that the experimental time series covers a substantially wider domain at small scales than the LES. This is the effect of the LES cutoff at the local grid scale. Case 19k-θH covers a wider range of scales than case 19k-θL (see Figures 5(c) and 5(d)) because of the smaller time step size dt. Although the position of the spectra maximum

Downloaded 22 Oct 2012 to 128.250.144.147. Redistribution subject to AIP license or copyright; see http://pof.aip.org/about/rights_and_permissions

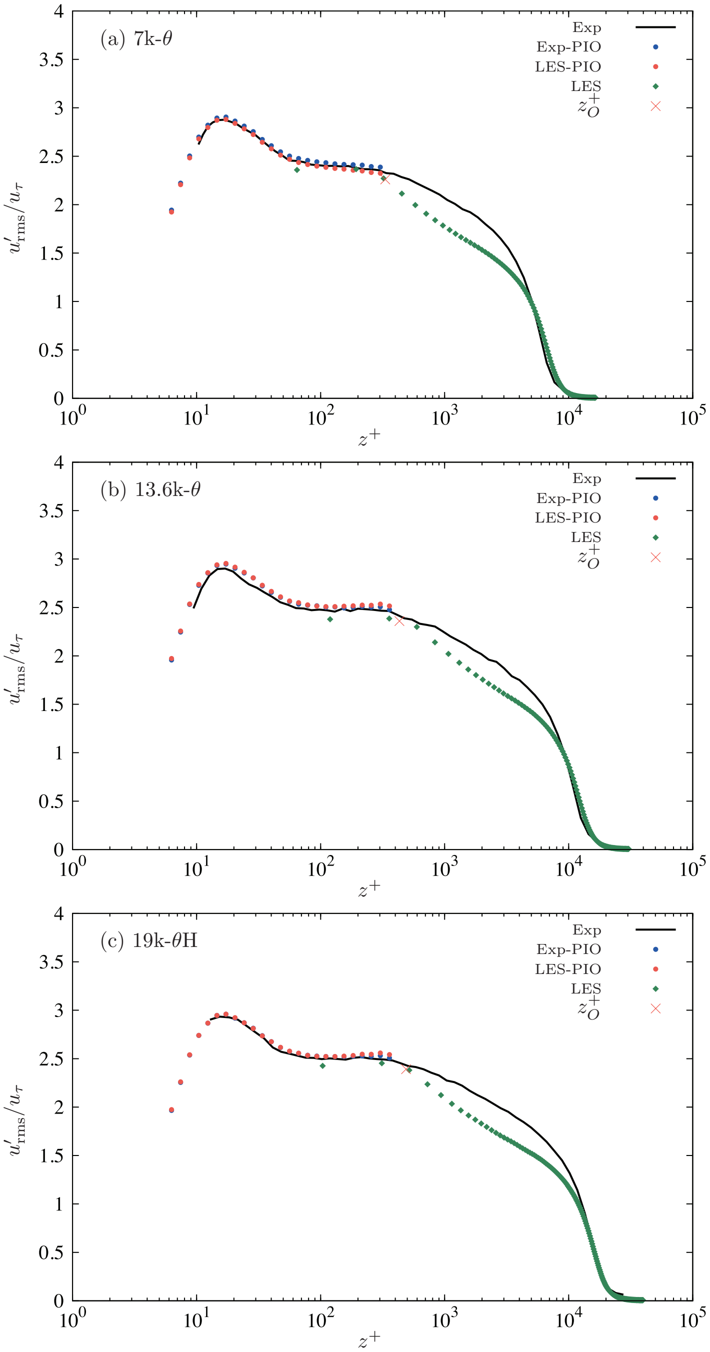

FIG. 4. Prediction of streamwise turbulence intensity u'_{rms}/u_τ as compared to measurements. Shown are direct experiment, direct LES and predictions of inner-layer intensities obtained using velocity signals from both experiment (Exp-PIO) and LES (LES-PIO). The symbol "×" marks the location where the time series $u_{OL}^+(t)$ is measured. (a) case 7k-θ; (b) case 13.6k-θ; and (c) case 19k-θH.

tends to be shifted toward smaller scales for the LES, the peak magnitude of LES and experiment are comparable. Importantly, the turbulent energy of the large-scale signal u_{OL}^+ – the areas under the curve on the right-hand side of the cut-off wavelength $\lambda_x^+ \geq 7000$ – remains close, only differing by a slight energy re-distribution. We recall that to extract u_{OL}^+ from the velocity signal taken from LES, the velocity signal u_O^+ is filtered to retain only large scales above streamwise wavelengths

Downloaded 22 Oct 2012 to 128.250.144.147. Redistribution subject to AIP license or copyright; see http://pof.aip.org/about/rights_and_permissions

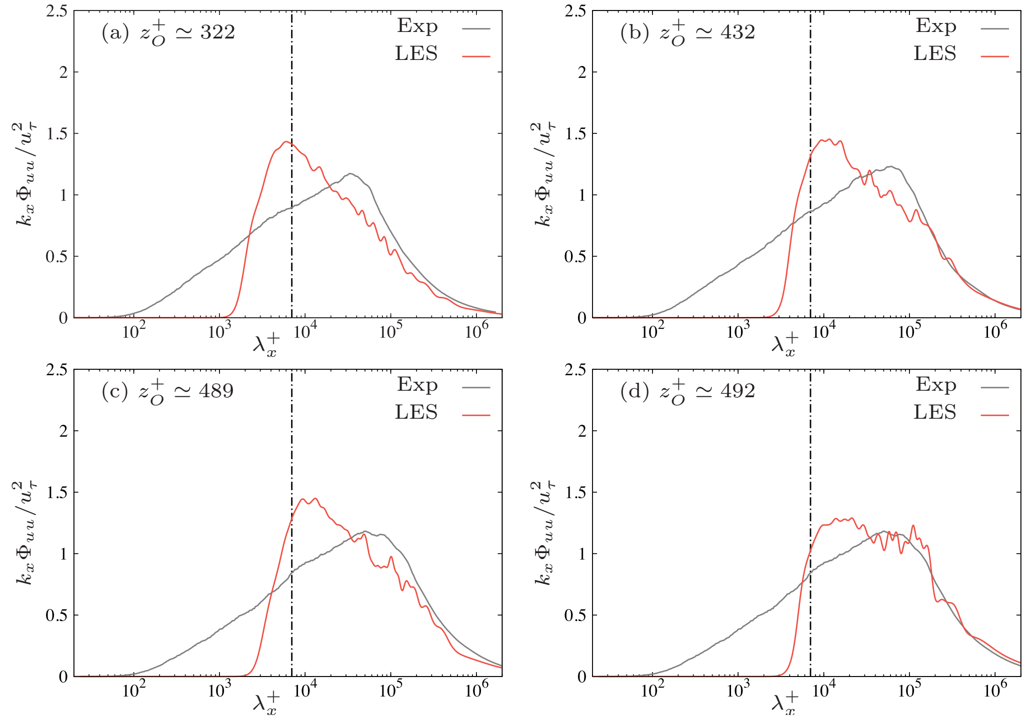

FIG. 5. Pre-multiplied energy spectra $k_x \Phi_{uu}/u_\tau^2$ at $z_O^+ \simeq \sqrt{15 Re_\tau}$ as compared to measurements; thick (red) lines: LES; thin (grey) solid lines: measurements.[7] (a) Case 7k-θ; (b) case 13.6k-θ; (c) case 19k-θH; and (d) case 19k-θL. The vertical dotted-dashed line shows the location of the cut-off wavelength, $\lambda_x^+ = 7000$.

of $\lambda_x^+ = 7000$. This constitutes another limiting factor for higher Reynolds number application of the current LES as it is necessary to take smaller *dt* as Reynolds number increases to fulfil this requirement.

The contour maps of predicted pre-multiplied energy spectra, $k_x \Phi_{uu}/u_\tau^2$, shown in Figure 6, indicate that the Reynolds number effects are well captured by the LES-PIO model. Particularly, the increasing large-scale energy content with increasing Re_τ. A closer view of the pre-multiplied energy spectra is given in Figure 7, at the inner-peak location $z^+ \simeq 15$ and for two Reynolds numbers, $Re_\tau = 7300$ and 19 000. Again, excellent agreement is observed. However, in Figures 6 and 7(a) distinct discontinuity or a hump is observed around $\lambda_x^+ \simeq 4000-7000$. This discontinuity is attributed to the fact that the model in Eq. (1) combines signals from two different data sources, LES and experiments, which are not synchronized together (even if the purpose of Fourier phase shift is to attempt to resolve this issue). Therefore, there is an overlap in the spectral domain between the universal signal $u*$ and the large-scale input component u_{OL}^+, which induces this discontinuity. There are also nonlinear effects in Eq. (1) arising from multiplying two time series with different spectral support. Nevertheless, this does not propagate nor does it contaminate other statistics due to the fact the discontinuity has a very low energy.

C. Signal length and resolution effects

To ensure that results are not sensitive to the signal length provided by LES, sensitivity tests were performed for all the cases using elongated velocity signals constructed from concatenation of signals from different spanwise locations. Spanwise locations were at least $2\delta_0$ apart to obtain uncorrelated signals. The results (not shown) do not make noticeable changes to the predictions. This is because the largest scales are already captured and converged in the time series obtained at a single location, allowed by the large computational domain used by the LES, $(L_x, L_y, L_z) = (72\delta_0, 6\delta_0, 4\delta_0)$.

Downloaded 22 Oct 2012 to 128.250.144.147. Redistribution subject to AIP license or copyright; see http://pof.aip.org/about/rights_and_permissions

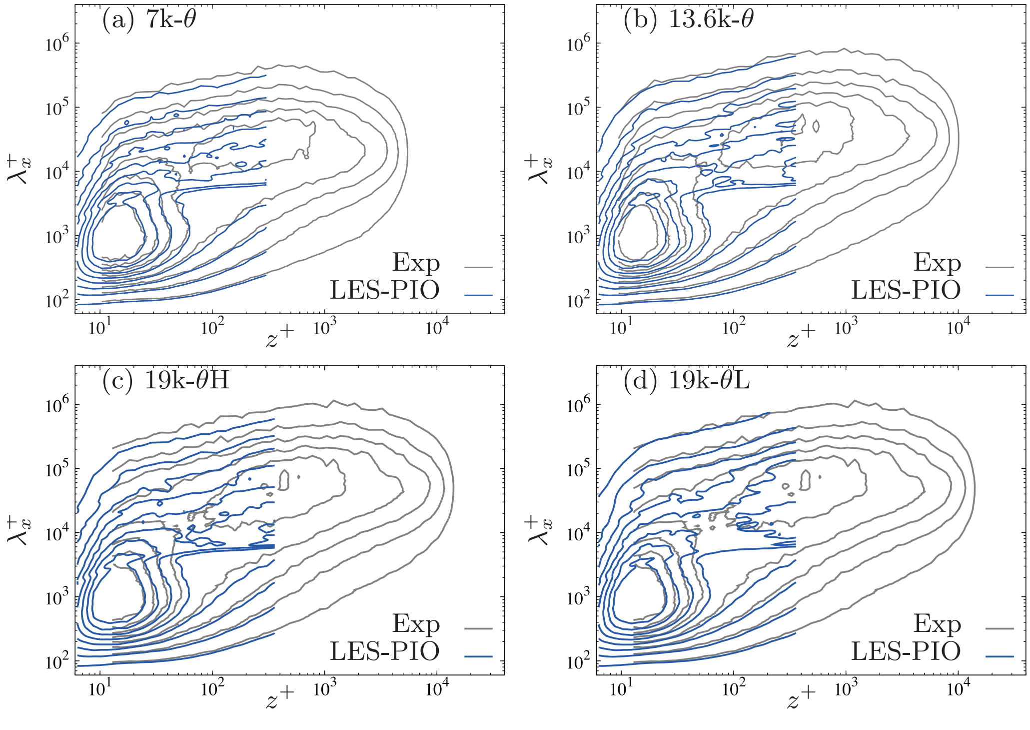

FIG. 6. Predicted pre-multiplied energy spectra map of the streamwise velocity fluctuations $k_x \Phi_{uu}/U_\tau^2$; thick (blue) lines: prediction from LES resolved velocity signal; thin (grey) solid lines: measurements.[7] (a) Case 7k-θ; (b) case 13.6k-θ; (c) case 19k-θH; and (d) case 19k-θL. Contours levels show $k_x \Phi_{uu}/U_\tau^2$ from 0.2 to 1.6 in steps of 0.2.

Figure 8 shows the effect of the LES grid's resolution on the predicted turbulent intensity profile at $Re_\tau = 19\,000$, for the low resolution case (19k-θL) and the high resolution case (19k-θH). The slightly larger prediction observed on the low resolution case is probably attributed to the LES containing more energy in the very long scales, compared to case 19k-θH as seen in Figures 5(c) and 5(d). Overall, the prediction from the higher resolution case 19k-θH agrees better with the experimental data. Recall that the grid position of z_O^+ is chosen to avoid the under-resolved region close to the virtual wall. The argument that numerical and modeling errors are unavoidable in the first few grid points was discussed in Cabot and Moin.[32]

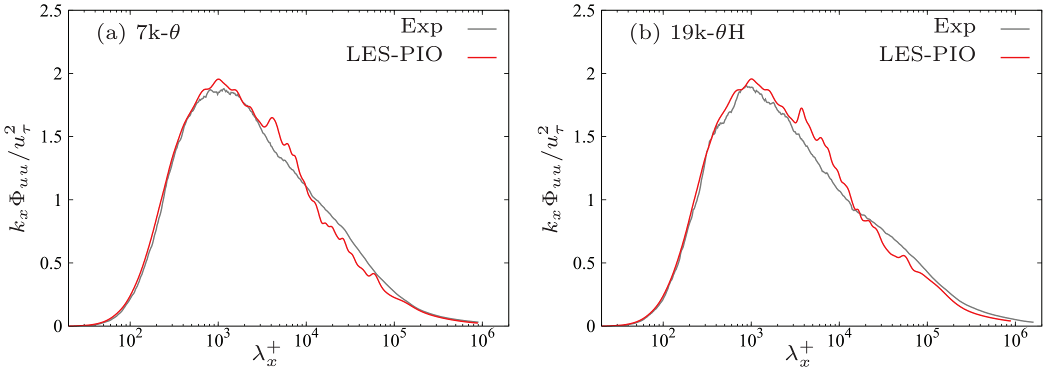

FIG. 7. Example of predicted pre-multiplied energy spectra $k_x \Phi_{uu}/u_\tau^2$ at the inner-peak location ($z^+ \simeq 15$) as compared to measurements; thick (red) lines: prediction from LES resolved velocity signal; thin (grey) solid lines: measurements.[7] (a) Case 7k-θ; and (b) case 19k-θH.

Downloaded 22 Oct 2012 to 128.250.144.147. Redistribution subject to AIP license or copyright; see http://pof.aip.org/about/rights_and_permissions

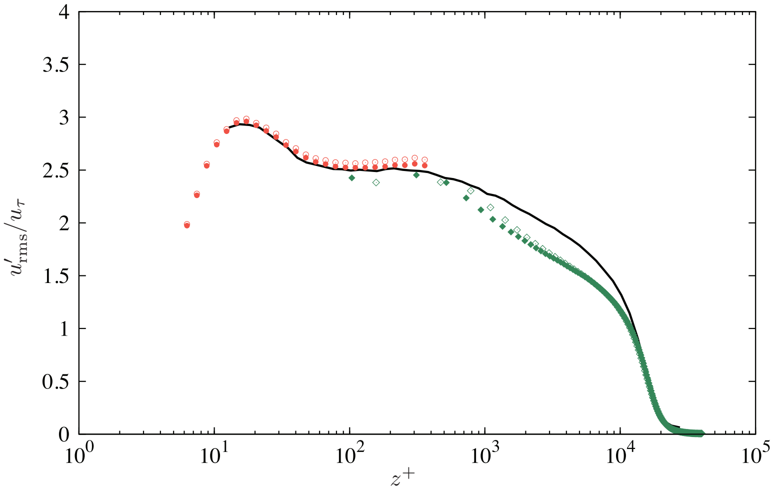

FIG. 8. The effect of resolution in LES-PIO predictions of streamwise turbulence intensity u'_{rms}/u_τ as compared to measurements. Also shown are intensities obtained directly from the LES, solid: case 19k-θH; open: case 19k-θL, and measurement at $Re_\tau = 19\,000$, solid line.

D. Measurement location and cut-off wavelength effects

As discussed in Sec. II A, the Reynolds number independent model parameters $u^*(z^+, t)$, $\alpha(z^+)$, and $\beta(z^+)$ are calibrated using filtered experimental measurement of the streamwise velocity signal taken from $z_O^+ = \sqrt{15 Re_\tau}$ with a cut-off wavelength $\lambda_x^+ = 7000$. Here, we performed sensitivity tests on the parameters z_O^+ and λ_x^+ using velocity signals from four other locations and using two other cut-off wavelengths, $\lambda_x^+ = 4000$ and $10\,000$ for case 19k-θH.

Results using the velocity signal from three locations in the range $105 < z_O^+ < 520$ (instead of $z_O^+ = \sqrt{15 Re_\tau} \approx 490$), corresponding to the first to the third computational grid point from the virtual wall, effectively show no discernible difference in LES-PIO prediction of turbulent intensity profiles (not shown) compared to the original prediction shown in Figure 4(c). Figure 9(a) shows LES-PIO prediction of turbulent intensity profiles using the signal from the fourth grid point, $z_O^+ \approx 730$. Although a deviation up to 2.9% at $z^+ \approx 200$ can be observed, the difference in predicted peak intensities at $z^+ \approx 15$ are smaller, of order 0.7%. Sensitivity to λ_x^+ is shown in Figure 9(b) which indicates some effects. This is expected since the model parameters are currently constructed for input of large-scale information with wavelength larger than $\lambda_x^+ = 7000$. Using $\lambda_x^+ = 4000$ and

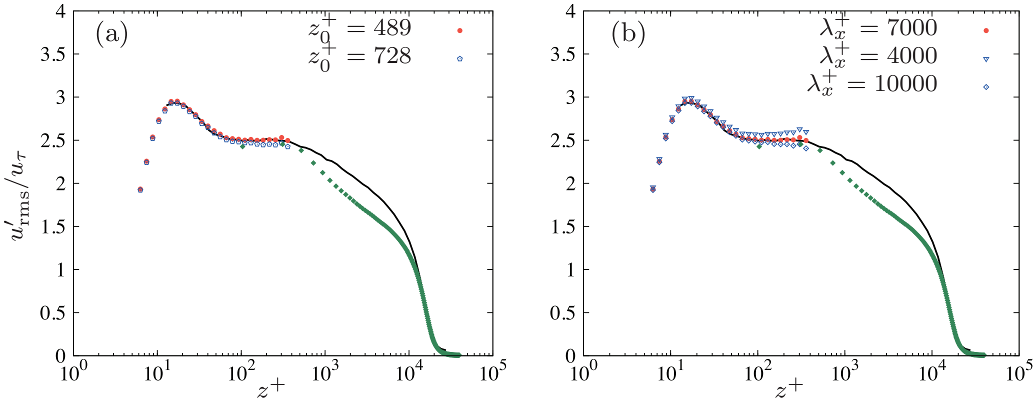

FIG. 9. The effect of z_O^+ and cut-off wavelength in LES-PIO predictions of streamwise turbulence intensity u'_{rms}/u_τ for case 19k-θH as compared to measurements. Also shown are intensities obtained directly from the LES, solid diamond, measurement at $Re_\tau = 19\,000$, solid line.

Downloaded 22 Oct 2012 to 128.250.144.147. Redistribution subject to AIP license or copyright; see http://pof.aip.org/about/rights_and_permissions

10 000 results in having more and less energy, respectively, within the predicted fluctuations. With proper calibrations for each cut-off value, the PIO model has been shown to be robust and exhibit little change with experimental velocity signal as an input. See Mathis *et al.* for details.[7]

V. RESULTS AT LARGER REYNOLDS NUMBER

A. Turbulence intensity and spectra

The combined LES-PIO model has been shown to fairly accurately reconstruct the near-wall field at intermediate Reynolds numbers. Particularly, a good agreement has been found with experiments and Exp-PIO predictions. Now we test the model at higher Reynolds numbers, $Re_\tau = 62\,000$, 100 000, and 200 000, filling the gap between laboratory and atmospheric surface layer data. It should be noted that at such high-Re_τ there is no experimental data available in the near-wall region for comparison, and outer-region data are only available for $Re_\tau = 62\,000$. Figure 10 depicts the predicted streamwise turbulent intensity profiles along with LES and experimental results. SLTEST data and corresponding Exp-PIO results have been included as an indicator of the predicted trends of turbulence intensity obtained from experiment. As discussed previously, the LES tends to underestimate the intensities in the outer part of the boundary layer, due to the missing small-scale energy content, but the essential Re_τ dependency feature is well captured. The magnitude of the LES-PIO intensity results at $Re_\tau = 62\,000$ are in good agreement with experiment, at least where the measurements and the prediction intersects. The SLTEST prediction, at $Re_\tau = 1.4 \times 10^6$ suggests that at high-Re_τ a second peak in the streamwise turbulent intensity profile emerges, and the LES-PIO results appear to support this. However, it should be recalled that the PIO model has been built using hot-wire measurements where a normalized sensor length, $l^+ = lu_\tau/\nu = 22$, was used. Therefore, $u*$ and u_p^+ in Eq. (1) have the same spatial resolution characteristic, and the emergence of the second peak might be a result of spatial resolution issues.[34,35] Nevertheless, the existence of an outer peak remains an open question. Based on the diagnostic plot,[36] Alfredsson *et al.*[15] suggested that an outer peak does exist at $z^+ = 0.81 Re_\tau^{0.56}$ if the Reynolds number is sufficiently large. For pipe flow, McKeon and Sharma[37] use a linear model to identify a dominant VLSM-like mode whose propagation velocity matches the local mean velocity at $z^+ \sim Re_\tau^{2/3}$. They argue that at this "critical layer," the exchange of energy between the mean flow and the forced mode is enhanced resulting in a peak in turbulence intensity. It should be noted that LES-PIO results shown in the present paper are up to $z^+ \approx 360$ and do not reach the proposed outer-peak location for cases 62k-τ to 200k-τ (respectively, $z^+ = 970$ and $z^+ = 1230$).

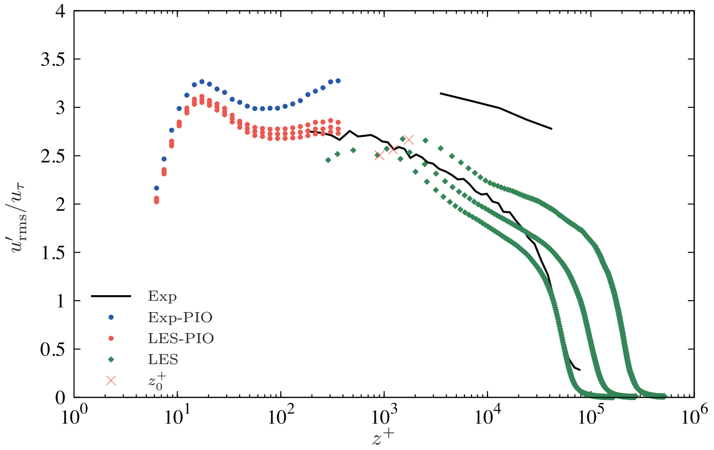

FIG. 10. Prediction of streamwise turbulence intensity u'_{rms}/u_τ for cases 62k-τ, 100k-τ, and 200k-τ. Also shown are measurements at $Re_\tau = 62\,000$ from Winkel *et al.*[24] and at $Re_\tau = 1.4 \times 10^6$ from SLTEST. The symbol "×" marks the location where the large-scale component is measured.

Downloaded 22 Oct 2012 to 128.250.144.147. Redistribution subject to AIP license or copyright; see http://pof.aip.org/about/rights_and_permissions

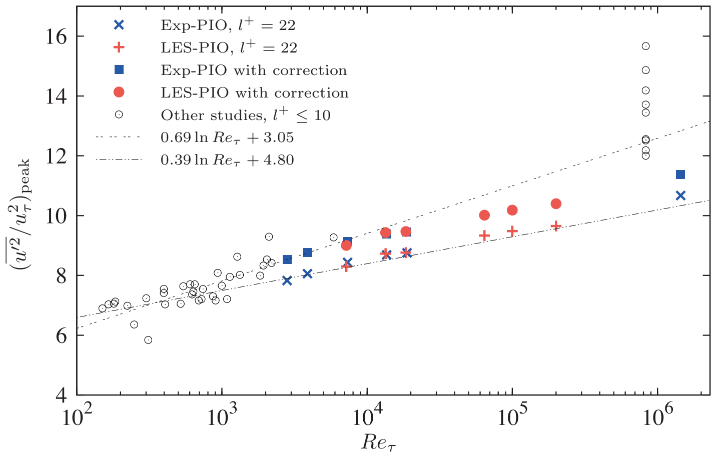

FIG. 11. Reynolds number dependency of the inner-peak intensity $\overline{u'^2}/u_\tau^2$ (around $z^+ = 15$) for Exp-PIO, LES-PIO and those with correction taking into account the hot-wire spatial resolution effect[33] to an assumed wire length of $l^+ = 3.8$; The open-circle symbols (◯) are a compilation of results from where $l^+ \leq 10$, including DNS and experimental measurements from channel flow, boundary layer, and atmospheric surface layer (see Hutchins and Marusic[6] for details).

Figure 11 shows the Reynolds number dependency of the near-wall peak in $\overline{u'^2}/u_\tau^2$, for Exp-PIO and all LES-PIO results, along with available data from the literature. Also included are the spatially corrected Exp-PIO and LES-PIO results using the correction scheme proposed by Chin *et al.*[33] to take into account the spatial resolution effects of the PIO model ($l^+ = 22$), where the missing energy is modeled using two-dimensional spectra from DNS of turbulent channel flow. Overall, the LES-PIO follows the general trends of both direct measurement and Exp-PIO and support loglike increase in $\overline{u'^2}/u_\tau^2$ with increasing Re_τ. In particular the three high-Reynolds number LES-PIO results are seen to fall within a large gap between laboratory and SLTEST estimates. Two empirical fits to the data are shown in Figure 11. The log-relation

$$\left(\frac{\overline{u'^2}}{u_\tau^2}\right)_{\text{peak}} = 0.39\ \log(Re_\tau) + 4.80 \tag{3}$$

has the same gradient proposed by Marusic *et al.*[38] using measurement with consistent l^+, whereas other studies presented different slopes.[6–8] We comment that experimental measurement of the logarithmic growth remains uncertain owing in part to variable hot-wire sensor size l^+ that can produce attenuation effects in the measured peak turbulent intensity: see Hutchins *et al.*[34] and Örlü *et al.*[39] for a review of measurement techniques and related issues. This potential source of uncertainty in our results is insignificant owing to the fact that our results are essentially equivalent of using constant hot-wire sensor size of $l^+ = 22$ and that they cover presently a wide range of Reynolds number.

The energy content of all LES-PIO prediction, for cases 7.3k-θ, 19k-θH, 62k-τ, and 200k-τ, are given in Figure 12 for the inner-peak location, $z^+ \simeq 15$. Again, it can be observed that the increasing large-scale energy with increasing Re_τ is well captured by the LES-PIO, identically to the Exp-PIO model shown in Mathis *et al.*[7]

B. Higher order statistics

Direct LES and LES-PIO results for skewness and kurtosis are shown compared with direct experimental measurement and also Exp-PIO results in Figure 13. The LES-PIO results show excellent agreement with experiment in the inner layer, while Exp-PIO and the LES-PIO results are indistinguishable. The results of direct LES in the outer layer are overall good up to the edge of boundary layer, except for a few grid points near the virtual wall. As in turbulent intensity prediction,

Downloaded 22 Oct 2012 to 128.250.144.147. Redistribution subject to AIP license or copyright; see http://pof.aip.org/about/rights_and_permissions

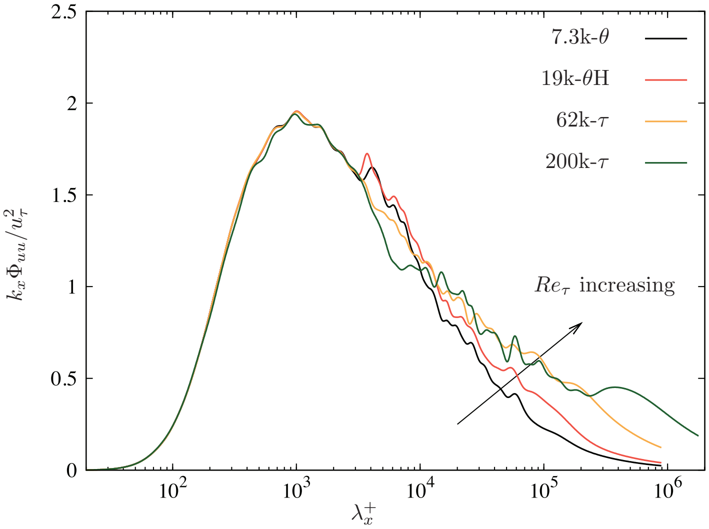

FIG. 12. Reynolds number evolution of the predicted pre-multiplied energy spectra $k_x\Phi_{uu}/u_\tau^2$ at the inner-peak location ($z^+ \simeq 15$) for cases 7.3k-θ, 19k-θH, 62k-τ, and 200k-τ.

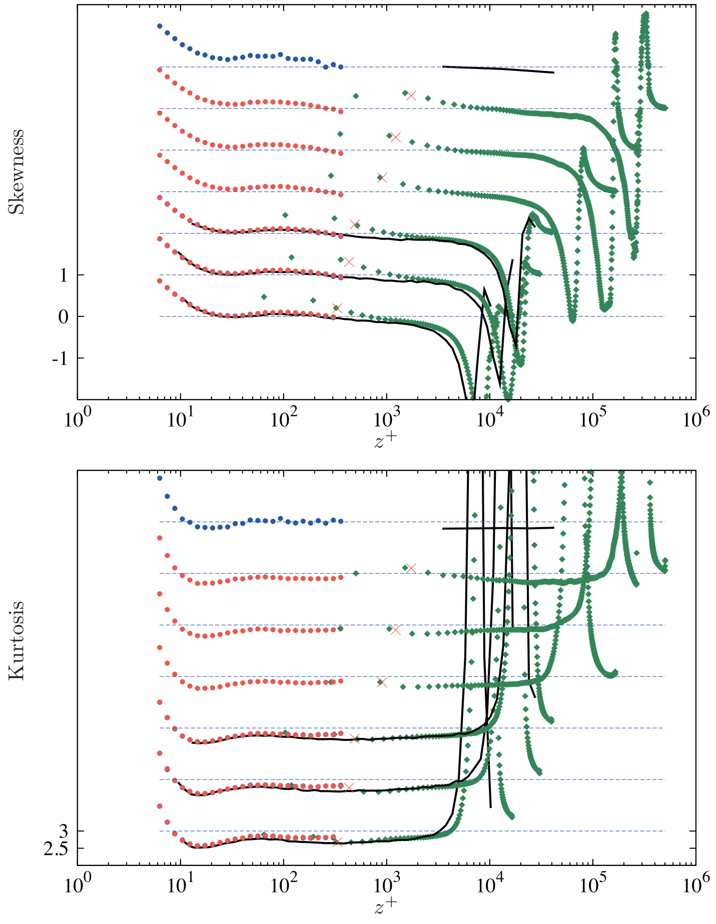

FIG. 13. Skewness $\overline{u'^3}/(\overline{u'^2})^{3/2}$ and Kurtosis $\overline{u'^4}/(\overline{u'^2})^2$ profile for cases 7.3k-θ, 13.6k-θ, 19k-θH, 62k-τ, 100k-τ, and 200k-τ. (From bottom to top) The experimental measurements at $Re_\tau = 7300$, 13 600, and 19 000 are from Mathis *et al.*[7] The highest Reynolds number case corresponds to SLTEST data. The symbol "×" marks the location of where the large-scale component is measured. For key see Figure 10.

Downloaded 22 Oct 2012 to 128.250.144.147. Redistribution subject to AIP license or copyright; see http://pof.aip.org/about/rights_and_permissions

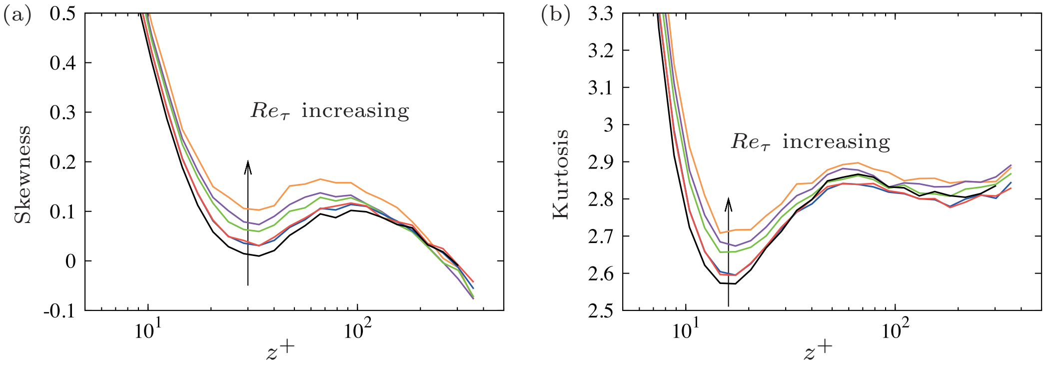

FIG. 14. Reynolds number dependency of predicted (a) skewness and (b) kurtosis using the LES-PIO model, for cases 7.3k-θ, 13.6k-θ, 19k-θH, 62k-τ, 100k-τ, and 200k-τ.

a discontinuity can be seen between the inner-layer LES-PIO results and the direct outer-layer LES results (see Figures 4 and 10). It should be noted that the PIO model does not guarantee that the predicted value should exactly match the actual value that the velocity signal itself has at $z^+ = z_O^+$. The velocity signal used as an input only contains the fluctuations of the larger scale components. In a LES context, the input signal is a resolved scale signal without a sub-grid contribution, while the numerical values shown as outer-layer LES calculation in each figure contain a sum of resolved and estimated sub-grid contributions ($\overline{u'^2} = \overline{\widetilde{u}'\widetilde{u}'} + \overline{T_{xx}}$, for example), Figure 14 shows the predicted LES-PIO skewness and kurtosis for all present Reynolds numbers. The small but definite Reynolds number dependency is clear. Such Reynolds number dependency of the third and fourth moments have previously been reported by Metzger and Klewicki,[8] arguing that this trend is caused by the growing influence of the large-scales with Re_τ. More recently, Mathis *et al.*[40] have shown that the increase in the skewness profile is closely related to an increasing effect of amplitude modulation with Re_τ, a nonlinear effect from large-scale signal rather than a simple superposition.[8] Our results indicate that this effect continues to grow.

VI. CONCLUSIONS

The present approach utilizes large eddy simulation[14,17] together with an inner-outer predictive model[7,12] to calculate the statistics of the fluctuating streamwise velocity in the inner region of the zero-pressure gradient turbulent boundary layer. The LES provides a time series of the streamwise velocity signal within the logarithmic region, which is then filtered and used as an input for the inner-outer predictive model to provide a streamwise fluctuating velocity within a region which is inaccessible to both the present LES (with a wall model) at all Reynolds numbers and present experimental measurements at very high Reynolds numbers.

We first tested the effectiveness of this approach at intermediate Reynolds number, $Re_\tau \sim 7300$, 13 600, and 19 000. This reproduced velocity fluctuations within the near-wall region, approximately $0 \leq z^+ < 360$, with reasonable agreement with direct experimental measurements for the streamwise turbulent intensities. Although small discontinuities are observed in the predicted pre-multiplied energy spectra map, the composite model captures the general trend of its energy distribution including the inner peak and a suggestion of the existence of outer peak in the wall-normal profile of turbulent intensities. It has also been shown that the deviations of the predictions from experiments are of the same order as those obtained using the velocity signal taken from experiments as input to the inner-outer predictive model. Time series obtained from the LES used as input to the inner-outer predictive model then provided predictions at the substantially larger Reynolds numbers of $Re_\tau = 62\,000$, 100 000, and 200 000. Further, higher order statistics comprising the skewness and kurtosis of the streamwise velocity fluctuations up to $Re_\tau \sim O(10^5)$ were also obtained and shown to give good agreement with experimental measurements at intermediate Reynolds numbers.

Downloaded 22 Oct 2012 to 128.250.144.147. Redistribution subject to AIP license or copyright; see http://pof.aip.org/about/rights_and_permissions

The LES appears to provide a large-scale velocity signal from the log-region that contains increasing energy in large-scale motions. As observed in the predicted pre-multiplied energy spectra profiles, the near-wall fluctuations contain an enhanced energy content in the large-scale motions with increasing Re_τ, which is consistent with previous experimental observations. Owing to this large-scale energy increase, the inner-peak turbulent intensity increases as $\log(Re_\tau)$. An increasing effect of amplitude modulation with Re_τ is also observed in the skewness profile. The LES-predictive inner-outer results support a loglike increase in the inner peak of the streamwise turbulence intensity with increasing Re_τ and provide prediction within a gap in $\log(Re_\tau)$ space between present laboratory measurements and surface-layer, atmospheric experiments. Overall, the LES appears to successfully capture the very large-scale motions that are hypothesized to drive this increase within the predictive inner-outer model.

Two principal advances of the present work can be summarized as follows: First, velocity time series obtained from LES and used as input to the inner-outer predictive model can be used to extend the wall-normal range of the LES well into the near-wall region. This has been demonstrated for the zero-pressure gradient, smooth-wall turbulent boundary layer, but the methodology appears sufficiently robust to be applicable to other wall-bounded turbulent flows such as pipe and channel flows and boundary layers in the presence of pressure gradients. Second, the results have provided predictions of the dependence of the near-wall peak in streamwise turbulent intensities that are beyond the range of present-day laboratory experimental facilities.

ACKNOWLEDGMENTS

This work was carried out with the financial support of the Australian Research Council.

[1] B. Ganapathisubramani, E. Longmire, and I. Marusic, "Characteristics of vortex packets in turbulent boundary layers," J. Fluid Mech. **478**, 35–46 (2003).
[2] J. del Álamo and J. Jiménez, "Spectra of the very large anisotropic scales in turbulent channels," Phys. Fluids **15**, L41–L44 (2003).
[3] C. Tomkins and R. Adrian, "Spanwise structure and scale growth in turbulent boundary layers," J. Fluid Mech. **490**, 37–74 (2003).
[4] K. Kim and R. Adrian, "Very large-scale motion in the outer layer," Phys. Fluids **11**, 417–422 (1999).
[5] N. Hutchins and I. Marusic, "Large-scale influences in near-wall turbulence," Philos. Trans. R. Soc. London, Ser. A **365**, 647–664 (2007).
[6] N. Hutchins and I. Marusic, "Evidence of very long meandering features in the logarithmic region of turbulent boundary layers," J. Fluid Mech. **579**, 1–28 (2007).
[7] R. Mathis, N. Hutchins, and I. Marusic, "A predictive inner–outer model for streamwise turbulence statistics in wall-bounded flows," J. Fluid Mech. **681**, 537–566 (2011).
[8] M. Metzger and J. Klewicki, "A comparative study of near-wall turbulence in high and low reynolds number boundary layers," Phys. Fluids **13**, 692 (2001).
[9] H. Abe, H. Kawamura, and H. Choi, "Very large-scale structures and their effects on the wall shear-stress fluctuations in a turbulent channel flow up to $Re_\tau = 640$," Trans. ASME, J. Fluid Eng. **126**, 835–843 (2004).
[10] A. Townsend, *The Structure of Turbulent Shear Flow*, 2nd ed. (Cambridge University Press, Cambridge, 1976).
[11] R. Mathis, N. Hutchins, and I. Marusic, "Large-scale amplitude modulation of the small-scale structures in turbulent boundary layers," J. Fluid Mech. **628**, 311–337 (2009).
[12] I. Marusic, R. Mathis, and N. Hutchins, "Predictive model for wall-bounded turbulent flow," Science **329**, 193 (2010).
[13] U. Piomelli, "Wall-layer models for large-eddy simulation," Prog. Aerosp. Sci. **44**, 437–446 (2008).
[14] M. Inoue and D. Pullin, "Large-eddy simulation of the zero pressure gradient turbulent boundary layer up to $Re_\theta = O(10^{12})$," J. Fluid Mech. **686**, 507–533 (2011).
[15] P. Alfredsson, A. Segalini, and R. Örlü, "A new scaling for the streamwise turbulence intensity in wall-bounded turbulent flows and what it tells us about the outer peak," Phys. Fluids **23**, 041702 (2011).
[16] P. Alfredsson, R. Örlü, and A. Segalini, "A new formulation for the streamwise turbulence intensity distribution in wall-bounded turbulent flows," Eur. J. Mech. B/Fluid (to be published).
[17] D. Chung and D. Pullin, "Large-eddy simulation and wall-modeling of turbulent channel flow," J. Fluid Mech. **631**, 281–309 (2009).
[18] J. Perot, "An analysis of the fractional step method," J. Comput. Phys. **108**, 51–58 (1993).
[19] Y. Morinishi, T. Lund, O. Vasilyev, and P. Moin, "Fully conservative higher order finite difference schemes for incompressible flow," J. Comput. Phys. **143**, 90–124 (1998).
[20] T. Lund, X. Wu, and K. Squires, "Generation of turbulent inflow data for spatially-developing boundary layer simulations," J. Comput. Phys. **140**, 233–258 (1998).
[21] J. Jewkes, Y. Chung, and P. Carpenter, "Modification to a turbulent inflow generation method for boundary-layer flows," AIAA J. **49**, 247–250 (2011).

Downloaded 22 Oct 2012 to 128.250.144.147. Redistribution subject to AIP license or copyright; see http://pof.aip.org/about/rights_and_permissions

[22] A. Perry, I. Marusic, and M. Jones, "On the streamwise evolution of turbulent boundary layers in arbitrary pressure gradients," J. Fluid Mech. **461**, 61–91 (2002).
[23] G. Oweis, E. Winkel, J. Cutbrith, S. Ceccio, M. Perlin, and D. Dowling, "The mean velocity profile of a smooth-flat-plate turbulent boundary layer at high Reynolds number," J. Fluid Mech. **665**, 357–381 (2010).
[24] E. Winkel, J. Cutbirth, S. Ceccio, M. Perlin, and D. Dowling, "Turbulence profiles from a smooth flat-plate turbulent boundary layer at high Reynolds number," Exp. Therm. Fluid Sci. **40**, 140–149 (2012).
[25] D. Chapman, "Computational aerodynamics development and outlook," AIAA J. **17**, 1293–1313 (1979).
[26] H. Choi and P. Moin, "Grid-point requirements for large eddy simulation: Chapmans estimates revisited," Phys. Fluids **24**, 011702–011702 (2012).
[27] H. Nagib, K. Chauhan, and P. Monkewitz, "Approach to an asymptotic state for zero pressure gradient turbulent boundary layers," Philos. Trans. R. Soc. London, Ser. A **365**, 755 (2007).
[28] M. P. Simens, J. Jiménez, S. Hoyas, and Y. Mizuno, "A high-resolution code for turbulent boundary layers," J. Comput. Phys. **228**, 4218–4231 (2009).
[29] K. Liu and R. Pletcher, "Inflow conditions for the large-eddy simulation of turbulent boundary layers: A dynamic recycling procedure," J. Comput. Phys. **219**, 1–6 (2006).
[30] B. Morgan, J. Larsson, S. Kawai, and S. Lele, "Improving low-frequency characteristics of recycling/rescaling inflow turbulence generation," AIAA J. **49**, 582–597 (2011).
[31] J. Brasseur and T. Wei, "Designing large-eddy simulation of the turbulent boundary layer to capture law-of-the-wall scaling," Phys. Fluids **22**, 021303 (2010).
[32] W. Cabot and P. Moin, "Approximate wall boundary conditions in the large-eddy simulation of high Reynolds number flow," Flow, Turbul. Combust. **63**, 269–291 (2000).
[33] C. Chin, N. Hutchins, A. Ooi, and I. Marusic, "Use of direct numerical simulation (DNS) data to investigate spatial resolution issues in measurements of wall-bounded turbulence," Meas. Sci. Technol. **20**, 115401 (2009).
[34] N. Hutchins, T. Nickels, I. Marusic, and M. Chong, "Hot-wire spatial resolution issues in wall-bounded turbulence," J. Fluid Mech. **635**, 103–136 (2009).
[35] I. Marusic, B. McKeon, P. Monkewitz, H. Nagib, A. Smits, and K. Sreenivasan, "Wall-bounded turbulent flows at high Reynolds numbers: Recent advances and key issues," Phys. Fluids **22**, 065103 (2010).
[36] P. Alfredsson and R. Örlü, "The diagnostic plot–a litmus test for wall bounded turbulence data," Eur. J. Mech. B/Fluids **29**, 403–406 (2010).
[37] B. McKeon and A. Sharma, "A critical-layer framework for turbulent pipe flow," J. Fluid Mech. **658**, 336–382 (2010).
[38] I. Marusic, R. Mathis, and N. Hutchins, "High reynolds number effects in wall turbulence," Int. J. Heat Fluid Flow **31**, 418–428 (2010).
[39] R. Örlü, J. Fransson, and P. Henrik Alfredsson, "On near wall measurements of wall bounded flows: The necessity of an accurate determination of the wall position," Prog. Aerosp. Sci. **46**, 353–387 (2010).
[40] R. Mathis, I. Marusic, N. Hutchins, and K. Sreenivasan, "The relationship between the velocity skewness and the amplitude modulation of the small scale by the large scale in turbulent boundary layers," Phys. Fluids **23**, 121702 (2011).

Downloaded 22 Oct 2012 to 128.250.144.147. Redistribution subject to AIP license or copyright; see http://pof.aip.org/about/rights_and_permissions